Study of the Effect of Annealing Temperature on the Structural and Optical Properties of ZnO Thin Films Prepared by Sol-Gel Method via Spin Coating

Abdullah Omar Ali [1]
Physics Department, Faculty of Science, University of Aden.

Mohsen Hussein Ahmed [2,*]
Physics Department, Faculty of Education, Saber, University of Laje
* Corresponding author. E-mail: mohssnhossean@gmail.com

DOI: https://doi.org/10.47372/jef.(2025)19.2.186

Abstract: This study investigated the effect of annealing temperatures (As -prepared, 350°C, 450°C, 550°C, and 650°C) on the properties of zinc oxide (ZnO) thin films prepared by sol-gel spin coating on glass substrates. X-ray diffraction (XRD) analysis confirmed a hexagonal wurtzite structure with an increase in grain size from 15 nm to 22 nm and a decrease in both residual stress and dislocation density with increasing annealing temperature. UV-Vis-NIR spectrophotometry measurements showed high transmittance in the visible region, a red shift in the transmittance edge, a decrease in film thickness from 333 nm to 280 nm, and an increase in refractive index, a decrease in the optical energy gap from 3.31 eV to 3.22 eV with increasing annealing temperature. while Urbach energy (E_U) exhibited non-linear behavior, reduced at 550 °C. Wemple-DiDomenico model fitting supported the improved crystallinity and reduced defects with increasing annealing temperature. Finally, the results showed an increase in free carrier density, increase plasma frequency with increasing annealing temperature.

Keywords: Zinc oxide thin films - X-ray diffraction- Optical energy gap- Urbach Energy- optical dispersion.

1. Introduction: Zinc oxide (ZnO) is a wide-bandgap semiconductor with a direct bandgap of approximately 3.37 eV at room temperature and a large exciton binding energy (60 meV) [1, 2]. Its properties make it suitable for a wide range of applications, including light-emitting diodes (LEDs), field-effect transistors, photovoltaic devices, room-temperature UV lasers, piezoelectric nanogenerators, and gas sensors [3]. ZnO nanoparticles, with their high specific surface area, exhibit defect states that significantly influence their optical and electrical properties [4]. While advanced vapor deposition techniques such as molecular beam epitaxy (MBE) [5], chemical vapor deposition (CVD) [6], metal-organic chemical vapor deposition (MOCVD) [7], and RF sputtering [8] have been used to grow ZnO films, these methods often suffer from drawbacks such as high cost, limited flexibility, and complex processing requirements. Solution-based deposition techniques, such as sol-gel [9] and spin-coating [10], offer attractive alternatives due to their simplicity, low cost, and ease of use. Furthermore, the influence of annealing on the structural and luminescent properties of ZnO thin films has been widely reported, resulting in enhanced performance [11].

This study systematically investigates the effects of varying annealing temperatures on the structural and optical properties of ZnO thin films prepared using the sol-gel spin-coating method. We characterize the crystalline structure, grain size, strain, dislocation density, optical transmittance, absorption, reflectivity, refractive index, energy gap energy, and Urbach energy as a function of annealing temperature using X-ray diffraction (XRD) and UV-Vis-NIR spectrophotometry. This comprehensive analysis aims to determine the optimal annealing conditions for producing high-quality ZnO thin films with superior optical and structural characteristics suitable for various applications. The results are further analyzed using established models, including the Debye-Scherrer equation, Williamson-Smallman formula, Swanepoel method, Wemple-DiDomenico model, Draud model, to provide a quantitative understanding of the annealing-induced modifications.

2. Experimental Details

2.1 Materials and Synthesis: Zinc oxide (ZnO) nanoparticles and thin films were synthesized using high-purity reagents: zinc chloride ($ZnCl_2$, 97.0–100.5% purity, Hi-LR™), sodium hydroxide (NaOH, ≥99.99% purity, Merck), acetic acid (CH_3COOH, ≥99.5% purity, Fisher Scientific), ethanol (C_2H_5OH, ≥99.8% purity, Sigma-Aldrich), and distilled water.

2.1.1 ZnO Nanoparticle Synthesis: 0.1 mol of zinc chloride ($ZnCl_2$) was dissolved in 100 mL of distilled water and stirred continuously using a magnetic stirrer. A solution of 0.2 mol of sodium hydroxide (NaOH) in 50 mL of distilled water was then slowly added to the zinc chloride solution while stirring at 60 °C . The mixture was stirred for 60 min to ensure complete precipitation of zinc hydroxide. Separate the zinc hydroxide from the solution using a centrifuge at 4000 rpm. The resulting zinc hydroxide precipitate was washed three times by distilled water and and two times by ethanol to remove any residual salts and unreacted precursors. The washed precipitate was then dried in an oven at 100 °C for 2 h and subsequently calcined at 300 °C for 1 h to obtain ZnO nanoparticles.

2.1.2 Colloidal Gel Preparation: 4.069 g of the synthesized ZnO nanoparticles were mixed with 10 mL of acetic acid in a glass flask and stirred continuously using a magnetic stirrer. 90 mL of ethanol was slowly added to the mixture, which was then stirred at 60 °C for 60 min. The resulting solution was incubated at room temperature for 24 h to form a stable colloidal gel.

2.2 ZnO Films Deposition: Glass substrates were cleaned sequentially with distilled water, methanol, and acetone to remove any impurities or dust. The colloidal gel was then spin-coated onto the substrates using a spin coater at 2000 rpm for 30 s. After each coating, the film was dried on a hot plate at 250 °C for 15 min to remove the organic binder and ensure strong adhesion to the substrate. This spin-coating process was repeated five times, with drying between each layer. Finally, the resulting ZnO films were annealed at 350 °C , 450 °C , 550 °C , and 650 °C for 60 min in a furnace to enhance their physical and chemical properties.

2. 3 Characterization of ZnO Films: The structural and optical characteristics of the ZnO thin films were investigated by X-ray diffraction (XRD) and UV-VIS-NIR spectrophotometer. XRD patterns were collected using a Bruker AXS D8 diffractometer with Cu Kα radiation (λ = 0.154056 nm) with a diffraction angle (2θ) ranging from 10° to 80°. Transmittance, absorption, and reflectivity spectra were obtained using a Jasco V-770 spectrophotometer over a wavelength range of 200–2500 nm. at a scanning speed of 1000 nm/min.

3. Results and Discussion:

3.1 Structural Analysis of ZnO Films: The structural properties of the ZnO thin films were investigated as a function of annealing temperature using X-ray diffraction (XRD). Figure (1) displays the XRD patterns of the as-prepared and annealed ZnO films at annealing temperatures of 350 °C , 450 °C , 550 °C , and 650 °C (annealing time: 60 minutes). The observed diffraction peaks at 2θ values of 31.61°, 34.39°, 36.11°, 47.40°, 56.52°, 62.72°, 66.29°, 67.91°, and 69.08°. These peaks correspond to the (100), (002), (101), (102), (110), (103), (200), (112), and (201) crystallographic planes of the hexagonal wurtzite structure (space group P63mc, JCPDS#36-1451) 12. The absence of additional peaks indicates the successful formation of ZnO crystals without significant impurity phases from the organic precursors or oxides. The presence of multiple peaks suggests a randomly oriented polycrystalline structure.

The sharp and well-defined diffraction peaks in Figure (1) indicate good crystallinity in the annealed films. A notable increase in the intensity of the (101) peak is observed with increasing annealing temperature, suggesting a preferred orientation along this plane during the annealing process. This preferential orientation may be related to oxygen vacancies within the ZnO crystal structure 13.

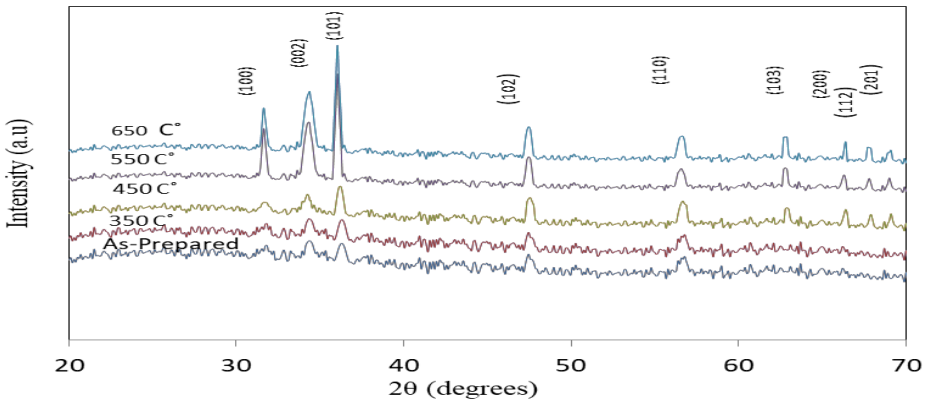

Figure 1 : X-ray diffraction patterns of annealed ZnO films at different temperatures.

3.1.1 Crystal Size (D), Strain (ε), and Dislocation Density (δ)

The crystallite size (D) was calculated from the most intense peak in the XRD patterns using the Debye-Scherrer equation 13:

$$D = \frac{K\lambda}{\beta_{hkl} COS\theta} \quad (1)$$

where D is the crystallite size (nm), K is the shape factor (typically ~0.9), λ is the X-ray wavelength (0.154056 nm), θ is the Bragg angle, and β_{hkl} is the full width at half maximum (FWHM) of the diffraction peak in radians. The dislocation density (δ), representing the number of defects per unit volume, was calculated using the Williamson-Smallman formula 16:

$$\delta = \frac{1}{D^2} \quad (2)$$

The microstrain (ε) was determined using the following relationship 15:

$$\varepsilon = \left[\frac{\lambda}{D\ COS\theta} - \beta\right]\frac{1}{tan\theta} \quad (3)$$

Values 2θ The estimated, the calculated FWHM, and the average crystal size of annealed samples at different temperatures are listed in the table (1). The results show an increase in crystallite size from 15 nm to 22 nm with increasing annealing temperature, confirming the presence of nanoparticles. The increase in crystallite size with annealing temperature is attributed to enhanced oxygen diffusion, promoting crystal growth and coalescence 13. The concomitant decrease in dislocation density and microstrain indicates a reduction in crystalline defects (oxygen vacancies), leading to improved crystallinity and higher-quality films at higher annealing temperatures17.

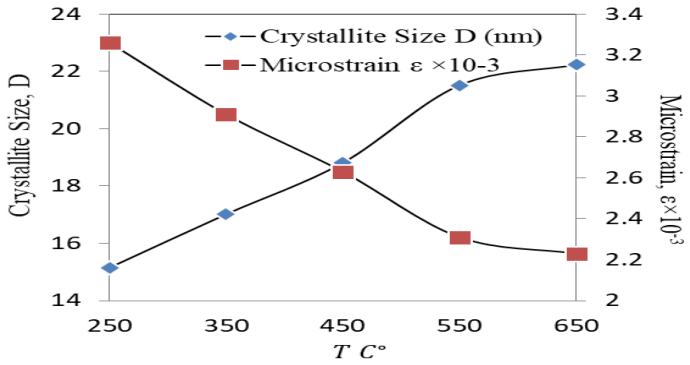

Figure 2 : Variation crystallite size *D* and microstrain *ε* of annealed zinc oxide films at different temperatures.

Table (1) also reveals a slight shift in the Bragg angle of the (101) plane towards lower values in the annealed samples compared to the as-prepared sample. This shift is attributed to the development of internal microstress. The observed peak broadening in the XRD data is a result of both crystallite size and microstrain. The decrease in microstrain with increasing annealing temperature suggests that atoms trapped in non-equilibrium positions during the synthesis process relax to more stable equilibrium positions upon annealing 14.

Table 1 : Crystal size (D), strain (ε), and dislocation density (δ) for ZnO films Annealed at different temperatures

Annealing Temperatures, °C	*2Θ degree*	*β(FWHM) degree*	*Crystallite Size, D, (nm)*	*Dislocation density, $\delta\times10^{15}$ (m^{-2})*	*Microstrain, $\varepsilon\times10^{-3}$*
As-Prepared	36.3015	0.551	15.15154	4.356	3.26
350 °C	36.3013	0.491	17.01602	3.454	2.91
450 °C	36.2010	0.444	18.81162	2.826	2.63
550 °C	36.1541	0.388	21.51357	2.161	2.31
650 °C	36.1535	0.375	22.23290	2.023	2.23

3.2 Optical Properties of ZnO Films: The optical properties of the ZnO thin films were characterized using UV-Vis-NIR spectrophotometry in the wavelength range of 300–2500 nm. Figure (3) illustrates the optical transmittance spectra as a function of wavelength for the as-prepared and annealed ZnO thin films at various temperatures (350, 450, 550, and 650°C). All deposited films exhibit high transparency within the visible and near-infrared regions, with an average transmittance exceeding 80% [1, 2].

A sharp decrease in transmittance is observed at wavelengths approximating 380 nm, corresponding to the fundamental absorption edge. This strong absorption is attributed to the direct transition of electrons from the valence band to the conduction band (band-to-band transition) [3]. Furthermore, the distinct oscillatory behavior (interference fringes) observed in the spectra indicates that the films possess smooth surfaces and good structural homogeneity, reflecting low surface scattering losses [4].

Regarding the effect of thermal treatment, a gradual enhancement in transmittance is observed as the annealing temperature increases up to 550°C. This improvement is ascribed to the enhancement of crystallinity and grain growth, which reduces the density of structural defects and impurities at grain boundaries, thereby minimizing light scattering and absorption centers within the film [5, 6]. However, upon further increasing the temperature to 650°C, a slight reduction in transmittance is noted. This behavior may be attributed to increased surface roughness resulting from excessive grain growth, which enhances surface scattering and consequently lowers the overall optical transmission [7].

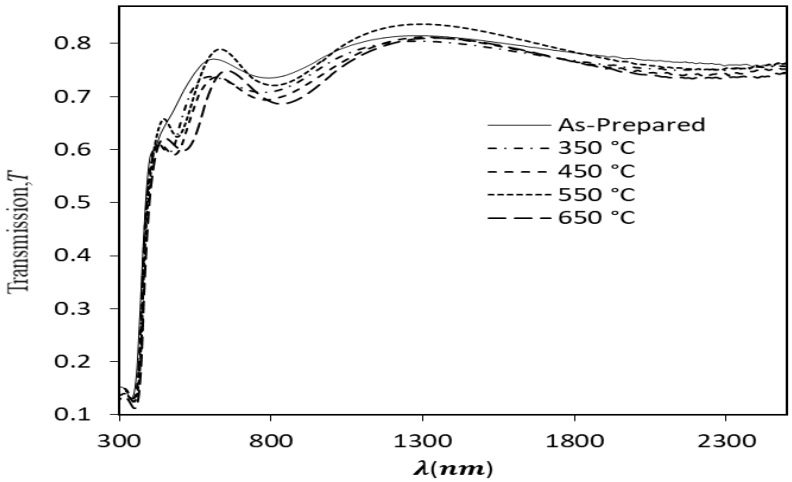

Figure 3 : Variation of transmittance spectrum with wavelength of annealed ZnO films at different temperature.

3.2.1 Calculation of thickness and refractive index of the ZnO Films

The thickness and refractive index of the deposited ZnO thin films were determined using Swanepoel's method 20, based on Manifacier's envelope method 21. This technique leverages the interference fringes observed in the optical transmittance spectra Figure (4) to extract these crucial film parameters.

Initially, the refractive index of the glass substrate (n_s) was calculated from its transmittance (T_s) using Eq. (4):

$$n_S = \frac{1}{T_S} + \left(\frac{1}{T_S^2} - 1\right)^{\frac{1}{2}} \quad (4)$$

This equation directly relates the substrate's refractive index to its transmittance, a well-established relationship for transparent substrates.

calculated using Equations (5) and (6):

$$n = \sqrt{\left[N + \sqrt{N^2 - n_S^2}\right]} \quad . \quad (5)$$

Where

$$N = \frac{2n_S(T_M - T_m)}{T_M T_m} + \frac{n_S^2 + 1}{2} \quad (6)$$

where T_M and T_m represent the maximum and minimum transmittance values obtained from the envelopes of the transmittance spectrum, respectively.

The precision of this first calculation of the refractive index is enhanced after evaluating **(**d**)**. The fundamental relation who gives the description of the interference fringes as shown in the following equation:

$$m = \frac{2nd}{\lambda} \quad . \quad (7)$$

This equation relates the order of interference (m), the refractive index (n), the thickness (d), and the wavelength (λ) , and (m) is an integer for the maximum values (or half an integer for the minimum values).

The film thickness (d) was obtained using Equation (8):

$$d = \frac{\lambda_1 \lambda_2}{2(\lambda_1 n_2 - \lambda_2 n_1)} \quad . \quad (8)$$

where λ_1 and λ_2 are the wavelengths corresponding to adjacent maximum (or minimum) transmittance values, and n_1 and n_2 are the respective refractive indices calculated using Equations (5) and (6). (Figure 4) This yielded an average thickness of approximately 333 nm for the as-prepared films. As shown in Table (2), annealing resulted in a thickness reduction (333 nm to 291 nm), attributed to the removal of residual organic matter and a consequent decrease in film porosity 22.

Further refinement of the refractive index was achieved by fitting the experimental data to the Cauchy relationship (Equation 9):

$$n = a + \frac{b}{\lambda^2} \quad . \qquad (9)$$

This allowed for extrapolation to wavelengths outside the range of experimental data. The constants 'a' and 'b' are determined from fitting the experimental data. As shown in Table (2), The resulting refractive index variation with wavelength (Figure 5) exhibits normal dispersion behavior, consistent with semiconductor materials. Importantly, annealing increased the refractive index, a consequence of improved crystallinity, increased crystallite size, reduced porosity, and increased density 23. This correlation is consistent with the Lorentz-Lorenz relationship 22 .

Finally, film porosity was calculated using the Lorentz-Lorenz equation (Equation 10)22:

$$Porosity\% = \frac{\rho_f}{\rho_b} = 1 - \left[\frac{[(n_f^2-1)/(n_f^2+2)]}{[(n_s^2-1)/(n_s^2+2)]}\right] \quad . \qquad (10)$$

where n_f is the refractive index of the porous ZnO films and n_s is the refractive index of the ZnO skeleton which is widely accepted as 2 .

Figure (6) depicts the variations of the porosity and the refractive index of the ZnO films as a function of annealing temperature. There, we found that the porosity of the films gradually decreases with increasing annealing temperature: a behaviour which provides a direct evidence for the correlation between the porosity and the refractive index of the ZnO films.

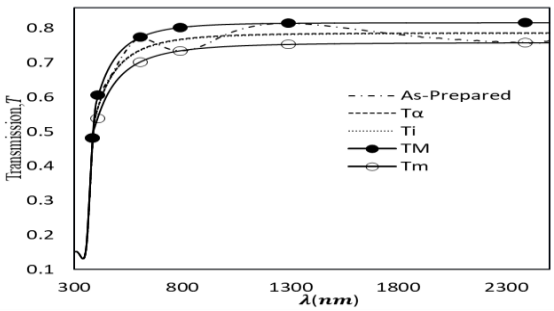

Figure 4 : Typical optical transmission spectrum for prepared thin ZnO films with constructed envelope curves.

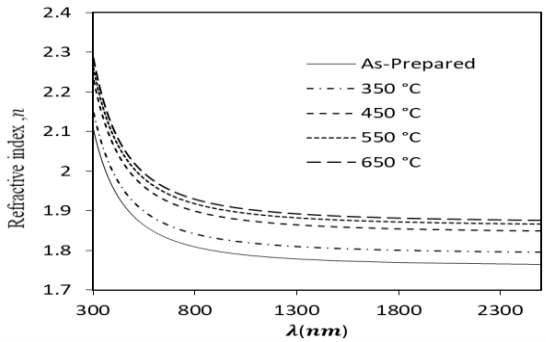

Figure 5 : Refractive index variation function in wavelength, for annealed ZnO at different temperatures.

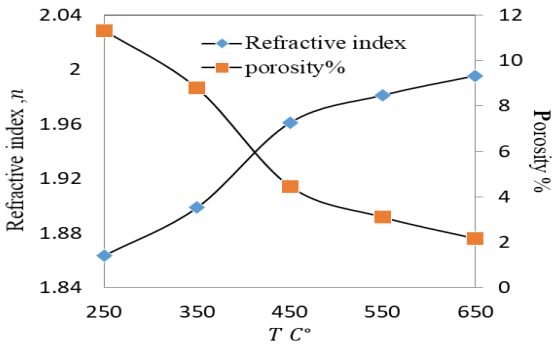

Figure 6: Variation of the refractive index at 550 nm and Porosity of ZnO films as a function of annealing temperature.

3.2.2 Absorption coefficient and The extinction coefficient

The absorption coefficient refers to the amount of light absorbed by a substance. The absorption coefficient (α) was calculated using the following formula25:

$$x = \frac{(E_M - \sqrt{(E_M^2 - (n^2-1)^3 (n^2 - n_s^4)})}{(n-1)^3 (n-n_s^2)} \quad . \qquad (a11)$$

$$E_M = \frac{8n^2 n_s}{T_M} + (n^2-1)(n^2-n_s^2) \quad . \qquad (b11)$$

Finally, the absorption coefficient is given by:

$$\alpha = -\frac{\ln(x)}{d} \quad . \qquad (c11)$$

where x is the absorbency and ***d*** is the thickness calculated from the equation (8). for each set of adjacent aphorisms or (minimas).

The extinction coefficient (k) was derived from the absorption coefficient using the relationship26:

$$k = \frac{\alpha\lambda}{4\pi} \quad . \qquad (12)$$

This coefficient reflects both absorption and scattering phenomena within the material, which are critical for understanding light behavior in thin films**.**

Figure (7) shows the change in absorption coefficient values as a function of photon energy (hν) of annealed thin ZnO films at different temperatures. By comparing the spectra of annealed samples at different temperature as shown in Figure (7) the absorption coefficient spectra of the thin ZnO films show a sharp absorption edge corresponding to the optical energy gap of the material. As the temperature increases through annealing, the absorption edge shifts towards lower energies (i.e. longer wavelengths) due to the thermal expansion of the crystal lattice 27.

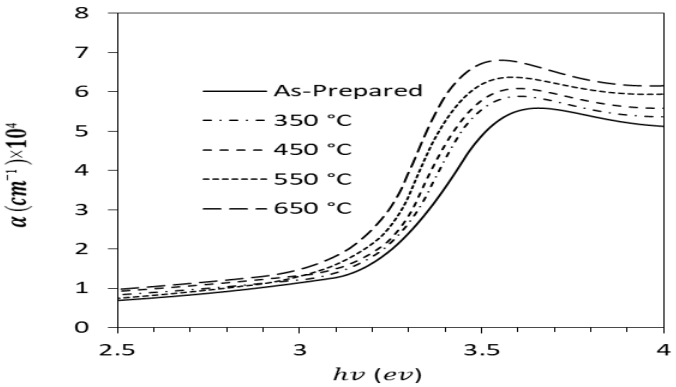

Figure 7: Absorption coefficient variation as a function of photon energy (hν) of annealed thin ZnO films at different temperature.

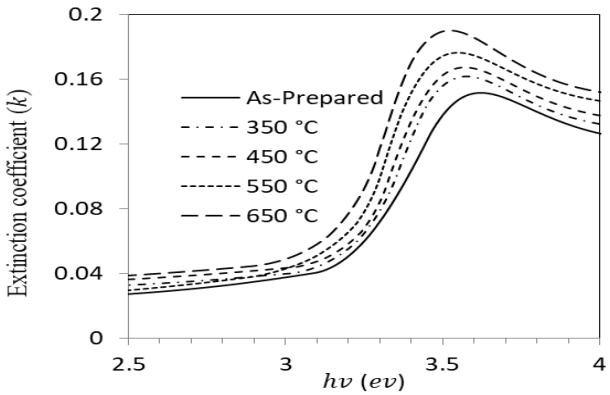

Figure 8: Variation of the Extinction coefficient as a function of photon energy (hν) of annealed ZnO films at different temperatures.

The extinction coefficient increased with photon energy, particularly in the high-energy region, where transitions from the valence band to the conduction band occur. As shown in Figure (8), the extinction coefficient values were minimal at lower photon energies, suggesting that the films remained relatively transparent. The increase in extinction coefficient with temperature suggests enhanced light trapping due to larger grain sizes, consistent with the findings of Mei et al. that attribute greater dispersion to larger grains27.

3.2.3 Optical Energy Gap amd urbach energy (E_U):

ZnO is a direct bandgap semiconductor. The optical energy gap E_g is determined using the Tauc relation (equation 13) 29:

$$\alpha h\upsilon = B\left(h\upsilon - E_g\right)^{\frac{1}{2}} \quad . \tag{13}$$

This equation is rearranged to:

$$(\alpha h\upsilon)^2 = B\left(h\upsilon - E_g\right) \quad . \tag{14}$$

Plotting (αhν)² versus hν (Figure 9) yields a straight line in the region near the band edge. Extrapolating the linear portion of this plot to the x-axis (where (αhν)² = 0) gives the value of E_g. The results indicate a decrease in energy gap (Eg) with increasing annealing temperature. The energy gap (Eg) for the as-prepared film was 3.306 eV, decreasing to 3.281 eV at 350 °C, 3.259 eV at 450 °C, 3.244 eV at 550 °C, and 3.22 eV at 650 °C. This near-linear decrease is attributed to increased grain size and improved crystallinity, reducing and the density of defect states within the bandgap 30, Furthermore, grain growth resulting from the increased annealing temperature contributes to decrease the energy gap. Larger grains reduce the surface area and associated surface defects, further contributing to decrease the energy gap (Eg) 31.

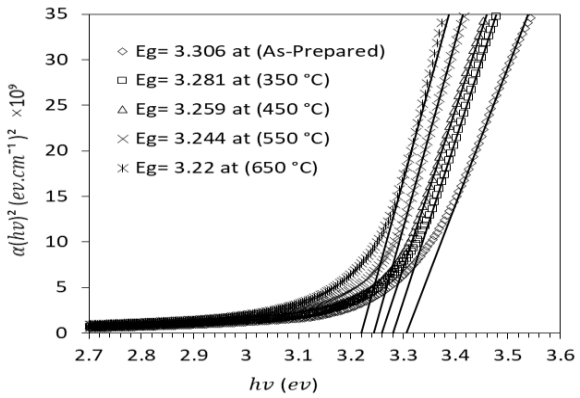

Figure 9 : Optical bandgap energies of ZnO films as a function of annealing temperature.

The Urbach energy (E_U), characterizing the width of the band tail states arising from disorder, was determined from the exponential region of the absorption edge. Equation (15) describes the Urbach tail 32:

$$\alpha = \alpha_0 \exp\left(\frac{(h\upsilon)}{E_U}\right) \quad . \tag{15}$$

Taking the natural logarithm of both sides (equation 14) yields a linear relationship:

$$ln(\alpha) = ln(\alpha_{0)}) + \frac{h\upsilon}{E_u} \quad . \tag{16}$$

Plotting ln(α) versus photon energy (hν) yields a linear relationship in the Urbach tail region (Figure 10), where the slope is inversely proportional to (E_U) [32].

Figure 10 presents ln(α) versus (hν) for annealed ZnO thin films, revealing a non-linear dependence of (E_U) on annealing temperature, indicative of significant microstructural evolution and defect density changes. The measured Urbach energies were, 0.282 eV for the as-prepared films, 0.384 eV at 350°C, 0.478 eV at 450°C, 0.419 eV at 550°C), and 0.525 eV at 650°C.

Critically, a significant reduction in (E_U) occurred at 550°C (0.419 eV) compared to 450°C (0.478 eV). However, (E_U) subsequently increased to 0.525 eV at 650°C. This non-monotonic variation in (E_U) correlates with annealing-induced structural changes.

At lower annealing temperature (350-450°C), high defect densities contribute to pronounced disorder, broadening the band tails and elevating (E_U) [2]. As annealing temperature increases to 550°C, enhanced atomic mobility facilitates defect annihilation and improved crystallinity, thereby reducing disorder and significantly

lowering (E_U) relative to 450°C 33. The subsequent rise in (E_U) at 650°C suggests the introduction of new defects, potentially due to thermally induced lattice strain or non-stoichiometry.

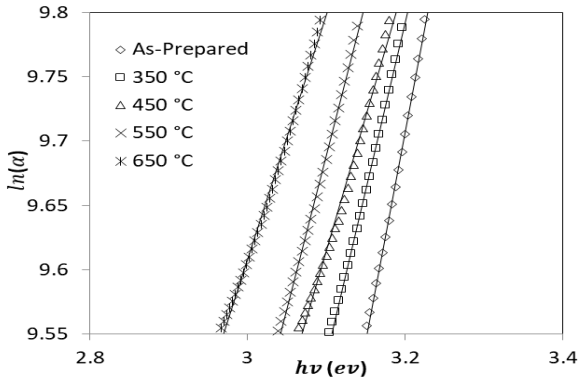

Figure 10 : Variance $\ln(\alpha)$ as a function of photon energy (hν) of annealed thin ZnO films at different temperature.

Complementary analysis (Figure 11) demonstrates the interdependence of the optical bandgap (E_g) and (E_U) with annealing temperature, both serving as indicators of structural disorder. The minimum (E_U) observed at 550°C highlights this temperature as optimal for mitigating disorder in this system. These results underscore the critical role of precise annealing temperature control in minimizing defect density and optimizing the optoelectronic quality of ZnO thin films [33]

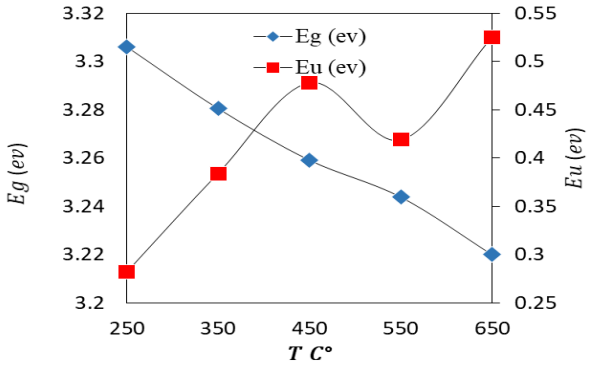

Figure 11 : Variation of optical energy gap and Urbach energy of ZnO films as a function of annealing temperature.

Table 2 : Optical parameters of ZnO films at different annealing temperatures.

Annealing Temperatures, °C	$n = a + \frac{b}{\lambda^2}$		$E_g(ev)$	$E_u(ev)$	*thickness nm*
	a	$b\times10^5\ nm^2$			
As-Prepared	1.760	0.313	3.306	0.282	333
350 °C	1.790	0.329	3.281	0.384	322
450 °C	1.843	0.357	3.259	0.478	303
550 °C	1.860	0.367	3.244	0.419	296
650 °C	1.870	0.380	3.220	0.525	291

3.2.4 The refractive index dispersion analysis: The dispersion of the refractive index was analyzed using the Wemple-DiDomenico model 34, which describes the electronic excitation spectrum below the absorption edge. The model is expressed as:

$$(n^2-1)^{-1} = \frac{E_0}{E_d} - \frac{E^2}{E_0 E_d} \quad . \qquad (17)$$

where n is the refractive index, E is the photon energy (hν), E_0 is the oscillator energy, and E_d is the dispersion energy. These parameters represent the energy of the effective oscillator and the average strength of interband optical transitions, respectively. Figure (12) shows a plot of $(n^2 - 1)^{-1}$ versus E^2. The slope and y-intercept yield values for E_0 and E_d. An approximation relating the oscillator energy to the optical energy gap (E_g) is $E_0 \approx 2E_g$.

Table (3) summarizes the obtained dispersion parameters. The dispersion energy (E_d) exhibited a significant positive correlation with annealing temperature. This increase is attributed to enhanced charge carrier (electron and hole) mobility within the ZnO lattice. Higher annealing temperatures promote increased charge carrier mobility, leading to more frequent interactions with lattice defects (vacancies and interstitials). This results in enhanced scattering, increasing (E_d). Furthermore, annealing-induced grain growth modifies the microstructure, particularly reducing grain boundary density and thus scattering centers, further contributing to the observed increase in (E_d) 36. These results highlight the crucial role of microstructural modifications in regulating charge carrier dynamics and optical dispersion 37.

Conversely, the oscillator energy (E_0) demonstrated a negative correlation with annealing temperature. This decrease reflects weakened Zn-O bond strength resulting from increased lattice vibrations at higher temperatures. The thermal energy imparted during annealing disrupts interatomic bonds, lowering the oscillator energy. Improved crystalline quality, characterized by reduced defect density and increased crystallite size, further contributes to the reduced (E_0) by diminishing the influence of defects on bond strength. The decreased (E_0) also indicates a reduction in the frequency of electron transitions, illustrating the impact of thermal processing on the ZnO film's electronic structure.

The static refractive index, n_0, was calculated using 35:

$$n_0^2 = 1 + \frac{E_o}{E_d} \quad . \qquad (18)$$

This increase in (n_0) is consistent with the observed improvements in crystallinity and material density, corroborating the trends observed in (E_0) and (E_d). The enhanced optical properties, reflected by the higher (n_0), are a direct consequence of the microstructural refinement and reduced defect density resulting from thermal annealing35.

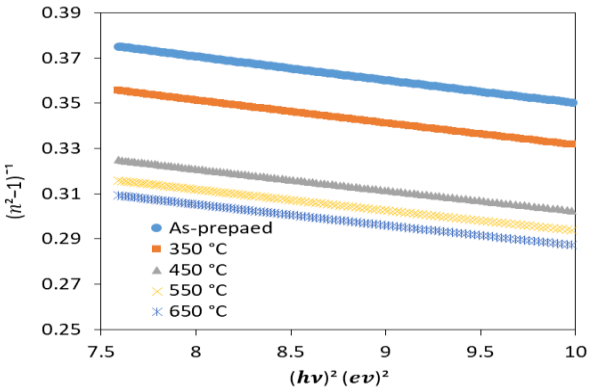

Figure 12: Variance between $(n^2 - 1)^{-1}$ and $(\mathbf{hv})^2$Annealed zinc oxide films at different temperatures.

Figure (13) illustrates the inverse relationship between (E_0) and (E_d), highlighting the interdependence of charge carrier mobility and crystalline lattice structure. The increase in (E_d) with annealing temperature, indicating enhanced charge carrier mobility, is coupled with a decrease in (E_0), reflecting weakened Zn-O bond strength. This inverse correlation, observed across the entire annealing temperature range, provides insights into the microstructural and electronic modifications induced by thermal processing. Reduced electron scattering and improved crystalline quality enhance the films' optical performance, as evidenced by the observed trends in (E_0) and (E_d) 36.

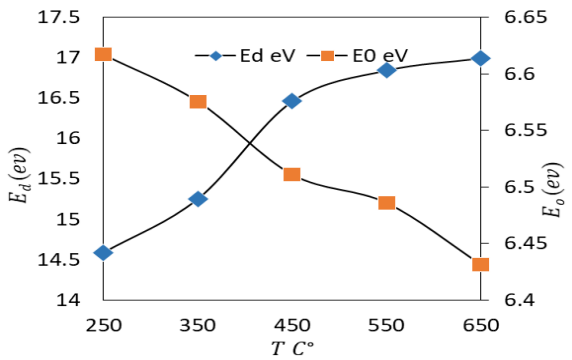

Figure 13: Variation of E_d and E_0 of annealed zinc oxide films at different temperatures.

The high-frequency dielectric constant ($\varepsilon_{\infty 1}$) was determined using a modified Drude model (Equation 19) 41:

$$\varepsilon_r = n^2 - k^2 = \varepsilon_{\infty 1} - \frac{1}{4\pi^2 c^2}\left(\frac{e^2 N}{\varepsilon_o m^*}\right)\lambda^2 \quad . \qquad (19)$$

where n and k are the refractive index and extinction coefficient, respectively. The analysis involved plotting ε_r against λ^2 (Figure 14).

Extrapolation to zero wavelength yields $\varepsilon_{\infty 1}$, while the slope provides N/m*, the ratio of free carrier concentration (N) to effective mass (m). Figure (14) shows The observed decrease in ε_r with increasing wavelength is consistent with reduced material response at longer wavelengths41.

The increase in $\varepsilon_{\infty 1}$ with annealing temperature is attributed to improved crystallinity and reduced defect density, leading to enhanced charge storage capacity42. This is further supported by the concurrent increase in N/m* with temperature (Figure 15), assuming m remains relatively constant43.

The plasma frequency, a measure of free carrier density, was calculated using (Equation 20) 43:

$$\omega_p = \left(\frac{e^2 N}{\varepsilon_{\infty 1}\varepsilon_o m^*}\right)^{\frac{1}{2}} \quad . \qquad (20)$$

The increase in ω_p with annealing temperature confirms the increased free carrier density observed in the ε_r[43]. Table (3) summarizes the dispersion parameters obtained at different annealing temperatures.

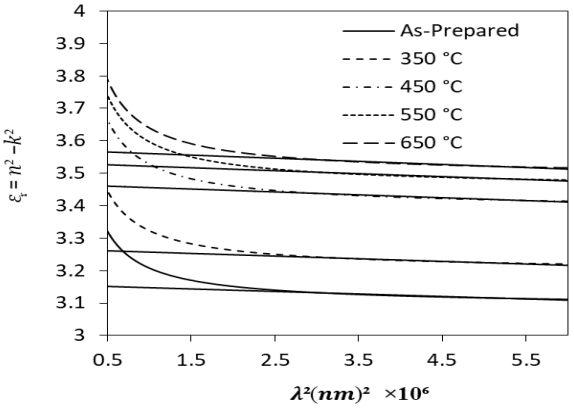

Figure 14: Variance between $\boldsymbol{\varepsilon_r}$ and$(\boldsymbol{\lambda})^2$ Annealed zinc oxide films at different temperatures.

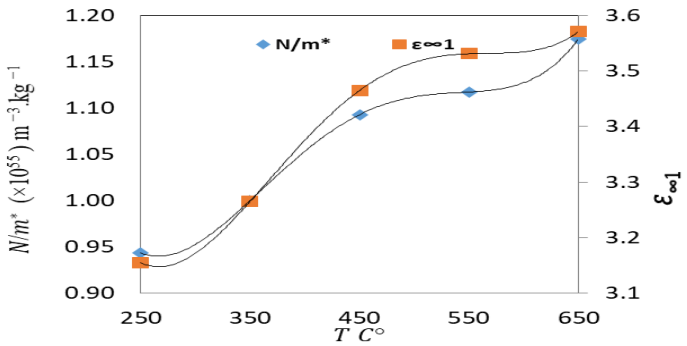

Figure 15: Variation of $\frac{N}{m^*}$ and $\boldsymbol{\varepsilon_{\infty 1}}$with increasing annealing temperature.

Table 3 : Dispersion parameters of ZnO films at different annealing temperatures:

Annealing Temperatures, °C	$E_o(ev)$	$E_d(ev)$	n_0	$\varepsilon_{\infty 2}$	$\varepsilon_{\infty 1}$	$N/m^*(\times 10^{55})$ $m^{-3}.kg^{-1}$	ω_P $(\times 10^{13})$ s^{-1}
As-prepared	6.617	14.589	1.790	3.205	3.155	0.944	9.312
350 °C	6.576	15.254	1.822	3.320	3.265	1.000	9.424
450 °C	6.511	16.460	1.878	3.528	3.465	1.093	9.563
550 °C	6.486	16.843	1.897	3.597	3.531	1.117	9.578
650 °C	6.431	16.993	1.908	3.642	3.570	1.174	9.766

Conclusions : This study aimed to investigate the effect of annealing temperature (As-prepared, 350°C, 450°C, 550°C, and 650°C) on the structural and optical properties of ZnO thin films prepared by sol-gel method and deposited by spin coating on glass substrates. X-ray diffraction (XRD) analysis confirmed a consistent hexagonal wurtzite structure across all samples, revealing enhanced crystallinity, increased grain size (15-22 nm), and reduced microstrain and dislocation density with increasing annealing temperature. UV-Vis-NIR spectrophotometry demonstrated high visible transmittance, a redshift in the transmittance edge, and thickness reduction (333-291 nm), attributed to improved crystallization and organic matter removal. A corresponding increase in refractive index reflected enhanced material density and crystal arrangement, The optical energy gap decreased (3.31-3.22 eV) with increasing annealing temperature, consistent with improved crystallinity and larger crystal size. Urbach energy exhibited a non-linear trend, reduced at 550 °C before a slight increase at 650 °C , suggesting optimal structural ordering at intermediate temperatures and the onset of defect formation at higher temperatures. Wemple-DiDomenico model analyses corroborated the improved crystal quality and reduced defects with increasing annealing temperature. Finally, enhanced free carrier density and improved optical dispersion properties were evidenced by increased plasma frequency with increasing annealing temperature.

References

1. Tzeng Lue, J., "Physical properties of nanomaterials", Encyclopedia of Nanoscience and Nanotechnology, Vol. X. H.S. Nalwa (Ed.), (2007), 1-46.
2. Özgür, Ü, Alivov, Y. I., Liu, C., Teke, A., Reshchikov, M. A., Dogan, S., Avrutin, V., Cho, S. J., Morkoç, H. "A comprehensive review of ZnO materials and devices", Journal of Applied Physics, Vol. 98, (2005), 041301-041301.
3. Al. -Kahlout, A., "ZnO nanoparticles and porous coatings for dye- sensitized solar cell application: Photoelectrochemical characterization", Thin Solid Films, Vol. 520, No. 6, (2012), 1814-1820.
4. Lin, B., Fu, Z. and Jia, Y., "Green luminescent center in undoped zinc oxide films deposited on silicon substrates", Applied Physics Letters, Vol. 79, No. 7, (2001), 943-945.
5. Ying, M., Wang, S., Duan, T., Liao, B., Zhang Y. and Mei, Z., "The structure, optical and magnetic properties of arsenic implanted ZnO films prepared by molecular beam epitaxy", Materials Letters, Vol. 171, (2016), 121-124.
6. Meng, X., Lin, B. and Fu, Z., "Influence of CH3COO– on the room temperature photoluminescence of ZnO films prepared by CVD", Journal of Luminescence, Vol. 126, No. 1, (2007), 203-206.
7. Pflitsch, C., Nebatti, A., Brors, G. and Atakan, B., "MOCVD- growth of thin zinc oxide films from zinc acetylacetonate and air," Journal of Crystal Growth, Vol. 348, No. 1, (2012), 5-9.
8. Purohit, A., Chander, S., Sharma, A., Nehra, S. P. and Dhaka, M. S., "Impact of low temperature annealing on structural, optical, electrical and morphological properties of ZnO thin films grown by RF sputtering for photovoltaic applications", Optical Materials, Vol. 49, (2015), 51-58.
9. Heidari, A., Zinatizadeh, A. A. L. and Younesi, H., "Controllable synthesis of flower-like ZnO nanostructure with hydrothermal method", International Journal of Engineering Transactions B: Applications, Vol. 22, No. 3, (2009), 283-290.
10. Dahnoun, M., Attaf, A., Saidi, H., Yahia, A. and Khelifi, C., "Structural, optical and electrical properties of zinc oxide thin films deposited by sol-gel spin coating technique," Optik - International Journal for Light and Electron Optics, Vol. 134, (2017), 53-59.
11. Kumar V., Kumar, V., Som, S., Yousif, A., Sigh, A., Ntwaeaborwa, O. M., Kapour A. and Swart, H. C., "Effect of annealing on the structural, morphological and photoluminescence properties of ZnO thin films prepared by spin coating", Journal of Colloid and Interface Science, Vol. 428, (2014), 8-15.
12. Cullity, B. D. and Stock, S. R. "Elements of X Ray Diffraction", 3rd ed., Prentice Hall, Upper Saddle River, NJ, 2001.
13. Tsoutsouva, M. G., Panagopoulos, C. N., Papadimitriou, D., Fasaki, I. and Kompitsas, M., "ZnO thin films prepared by pulsed laser deposition", Materials Science and Engineering: B, Vol. 176, No. 6, (2011), 480-483.

14. Khorsand Zak, A., Abd. Majid, W. H., Abrishami M. E. and Yousefi, R., "X-ray analysis of ZnO nanoparticles by Williamson–Hall and size–strain plot methods", Solid State Sciences, Vol. 13, No. 1, (2011), 251-256.
15. S. B. Qadri, E. F. Skelton, D. Hsu, A. D. Dinsmore, J. Yang, H. F. Gray, B. R. Ratna, Phys. Rev. B 60 (1999) 9191-9193.
16. S. Venkatachalam, D. Mangalaraj, Sa. K. Narayandass, Physica B 393 (2007) 47-55.
17. G. B. Williamson, R. C. Smallman, Phil. Mag. 1 (1956) 34-46.
18. V.Vasu,A.Subrahmaniam,Thin Solid Films Vol 113-194,1990..
19. Hussein 1H.F.,Ghufran Mohammad Shabeeb2, S.Sh. Hashim3. Preparation ZnO Thin Film by using Sol-gel-processed and determination of thickness and study optical properties. J. Mater. Environ. Sci. 2 (4) (2011) 423-426
20. Swanepoel, R.: Determination of the thickness and optical constants of amorphous silicon. J. Phys. E: Sci. Instrum. 16, 1214 (1983).
21. Manifacier, J.C., Gasiote, J., Fillard, J.P.: A simple method for the determination of the optical constants n, k and the thickness of a weakly absorbing thin film. J. Phys. E:Sci. Instrum. 9, 1002 (1976)
22. M. Ashraf, S. M. J. Akhtar, A. F. Khan, Z. Ali, A. Qayyum, J. Alloys. Compd. 509 (2011)2414-2419.
23. C. Baban, G. I. Rusu, P. Prepelita, Journal of Optoelectronics and Advanced Materials Vol. 7, No. 2, April 2005, p. 817-821.
24. R.K. pan, H. Z. Tao , H. C. Zang, T. J. Zhang, X. J. Zhao,Physica B, 404 (2009) 3397-3400.
25. Abdel-Galil, A., Moussa, N.L., Yahia, I.S.: Synthesis and optical characterization of nanocrystalline fluorine-doped tin oxide films: conductive window layer for optoelectronic applications Appl. Phys. A 127, 474 (2021).
26. X.. Zhang, J. Oin, Y. Xue, P. Yu, B. Zhang, L. Wang, and R. Liu. Effect of aspect ratio and surface defects on the photocatalytic activity of ZnO nanorods. 4596. doi:101038/srep04596, 2014.
27. Hapke, B., Theory of Reflectance and Emittance Spectroscopy. Cambridge University Press: New York, 2012.
28. Schneider, C. A.; Rasband, W. S.; Eliceiri, K. W., NIH Image to ImageJ: 25 years of image analysis. Nat. Methods 2012, 9, 671-675.
29. S. Ubaidillah, E.J. Wibawa, P. Bayu, P. and Agus Physical Characteristics of ZnO nanorods synthesized by low power DC thermal plasma, 2012. [13] Skoog et al.. "Principles of Instrumental Analysis". 6th edition. Thomason Brooks. Pp. 169-173, 2007.
30. Singh, R.G., Singh, F., Kumar, V. and Mehra, R. M., "Growth kinetics of ZnO nanocrystallites: Structural, optical and photoluminescence properties tuned by thermal annealing", *Current Applied Physics*, Vol. 11, (2011), 624-630.
31. Mahmood, A., Ahmed, N., Raza, Q., Khan, T. M., Mehmood, M., Hassan, M and Mahmood N., "Effect of thermal annealing on the structural and optical properties of ZnO thin films deposited by the reactive e-beam evaporation technique", *Physica Scripta*, Vol. 82, No. 6, (2010), 065801.
32. T. Olorunyolemi, Y. Birnboim, O. C. Carmel, J. R. Wilson, and I. K. Lloyd. Investigation of Structural and Optical Properties of Nano-crystaline ZnO J. Am. Ceram. Soc. 84, 2002.
33. A.J. Hashim∗, M.S. Jaafar, Alaa J. Ghazai, N.M. Ahmed, Fabrication and characterization of ZnO thin film using sol–gel method, Optik, Vol. 124, pp. 491–492, 2013.
34. A. Kashuba, H. Ilchuk, R. Petrus, I. Semkiv, O. Bovgyra, M. Kovalenko, V. Dzikovskyi, Modern Phys. Lett. B35, 2150189 (2021).
35. Sahai, A. and Goswami, N., "Structural and vibrational properties of ZnO nanoparticles synthesized by the chemical precipitation method", Physica E, Vol. 58, (2014), 130-137.
36. S. H. Wemple, M. DiDomenico, Phys. Rev., 3 (1971) 1338.
37. Yakuphanoglu, F.; Cukurovali, A.; Yilmaz, I. Single-oscillator model and determination of optical constants of some optical thin film materials. Phys. B Condens. Matter 2004, 353, 210–216.

38. Abd-ElrahmanMI,HafizMM, Abdelraheem AMand Abu-Sehly A A 2015 Characterization of optical constants and dispersion parameters of highly transparent Ge20Se76Sn4 amorphous thin film Opt. Mater. 50 99–103
39. Narayanan, G. N, Sankar Ganesh, R. and Karthigeyan, A., "Effect of annealing temperature on structural, optical and electrical properties of hydrothermal assisted zinc oxide nanorods", Thin Solid Films, Vol. 598, (2016), 39-45.
40. F. Yakuphanoglu, C. Viswanthan, J. Non-Cryst. Solids 353(2007) 2934-2937.
41. Singh, R.G., Singh, F., Kumar, V. and Mehra, R. M., "Growth kinetics of ZnO nanocrystallites: Structural, optical and photoluminescence properties tuned by thermal annealing", Current Applied Physics, Vol. 11, (2011), 624-630.
42. A.M. Alsaad, A.A. Ahmad, Q.M. Al-Bataineh, A.A. Bani- Salameh, H.S. Abdullah, I.A. Qattan, Z.M. Albataineh, A.D. Telfah, Materials 13, 1737 (2020).
43. I.S. Yahia, A.A.M. Farag, M. Cavas, F. Yakuphanoglu, Super- lattice. Microst. 53, 63 (2013).

دراسة تأثير درجة حرارة التلدين على الخصائص الهيكلية والبصرية لأفلام ZnO الرقيقة المحضرة بطريقة السول-جل بواسطة الطلاء الدوراني

عبد الله عمر علي[1]
قسم الفيزياء - كلية العلوم – جامعة عدن

محسن حسين أحمد[2]
قسم الفيزياء - كلية التربية - صبر – جامعة لحج

الملخص: هدفت هذه الدراســة إلى التحقيق في تأثير درجة حرارة التلدين (قبل المعالجة ،350،450 550،650 درجة مئوية)على خواص أفلام أكسيد الزنك (ZnO) الرقيقة المحضـرة بطريقة السـول-جل بواسـطة الطلاء الدوراني على ركائز زجاجية .أكد تحليل حيود الأشـعة السينية (XRD) وجود بنية بلورية سداسية من نوع wurtzite مع زيادة في حجم الحبوب من 15 نانومتر إلى 22 نانومتر، وانخفاض في كل من الإجهاد وكثافة الخلع مع ارتفاع درجة حرارة التلدين .أظهرت قياسـات الطيف الضـوئي في منطقة الأشـعة فوق البنفسـجية والمرئية والقريبة من الأشـعة تحت الحمراء (UV-Vis-NIR) نفاذية عالية في المنطقة المرئية، وانزياح أحمر لحافة النفاذية ، وانخفاض في سـمك الفيلم من 333 نانومتر إلى 291 نانومتر، وزيادة في معامل الانكسار، وتناقص في فجوة الطاقة البصرية من (3.31 -3.22 الكترون فولت) مع ارتفاع درجة حرارة التلدين. بينما أظهرت طاقة أورباخ (E_U) سلوكًا غير خطي، حيث انخفضت عند 550 درجة مئوية . دعمت تحليلات نموذج ويمبل-دي دومينيكو تحسـن جودة البلورة وانخفاض العيوب مع ارتفاع درجة حرارة التلدين .أخيرًا، أظهرت النتائج زيادة في كثافة الحاملات الحرة ، وتردد البلازما عند درجات حرارة التلدين الأعلى.

الكلمات المفتاحية: أغشية أكسيد الزنك الرقيقة - حيود الأشعة السينية - فجوة الطاقة البصرية - طاقة أورباخ - التشتت البصري.